



CHORUS

This is the accepted manuscript made available via CHORUS. The article has been published as:

Predicting the band gap of ternary oxides containing $3d^{\{10\}}$ and $3d^{\{0\}}$ metals

J. A. McLeod, A. Moewes, D. A. Zatsepin, E. Z. Kurmaev, A. Wypych, I. Bobowska, A. Opasinska, and S. O. Cholakh

Phys. Rev. B **86**, 195207 — Published 19 November 2012

DOI: [10.1103/PhysRevB.86.195207](https://doi.org/10.1103/PhysRevB.86.195207)

Predicting the Band Gap of Ternary Oxides containing $3d^{10}$, $3d^0$ Metals

J. A. McLeod and A. Moewes

*Department of Physics and Engineering Physics, University of Saskatchewan,
116 Science Place, Saskatoon, Saskatchewan S7N 5E2, Canada**

D. A. Zatsepin

*Institute of Metal Physics, Russian Academy of Sciences-Ural Division, 620990 Yekaterinburg, Russia and
Ural Federal University, 620002 Yekaterinburg, Russia*

E. Z. Kurmaev

Institute of Metal Physics, Russian Academy of Sciences-Ural Division, 620990 Yekaterinburg, Russia

A. Wypych, I. Bobowska, and A. Opasinska

Department of Molecular Physics, Technical University of Lodz, Lodz, Poland

S. O. Cholakh

Ural Federal University, 620002 Yekaterinburg, Russia

(Dated: today)

We present soft X-ray spectroscopy measurements and electronic structure calculations of ZnTiO_3 , a ternary oxide that is related to wurtzite ZnO and rutile TiO_2 . The electronic structure of ZnTiO_3 was calculated using a variety of exchange-correlation functionals, and we compare the predicted band gaps of this material obtained from each functional with estimates from our experimental data and optical gaps quoted from the literature. We find that main hybridizations in the electronic structure of ZnTiO_3 can be predicted from the electronic structures of the two binary oxides. We further find that ZnTiO_3 has weaker O $2p$ - Zn $3d$ repulsion than in ZnO , resulting in a relatively lower valence band maximum and consequently a larger band gap. Although we find a significant core hole shift in the measured O K XAS of ZnTiO_3 , we provide a simple empirical scheme for estimating the band gap that may prove to be applicable for any d^{10} - d^0 ternary oxide, and could be useful in finding a ternary oxide with a band gap tailored to a specific energy.

I. INTRODUCTION

Titanium dioxide (TiO_2) is currently one of the most important semiconductors since it has a high photocatalytic activity, is non-toxic, is stable in an aqueous solution, and is relatively inexpensive.^{1,2} Catalytic processes based on photoexcited electron-hole pairs can give rise to redox reactions with species adsorbed on the surface of the TiO_2 catalysts, and therefore TiO_2 has the potential to assist in water splitting.³ This material, however, has two main drawbacks during the photocatalytic process: (i) a large band gap (3.03 eV for rutile⁴ and 3.2 eV for anatase⁵) limits photocatalysis to only about 4% of the solar spectrum and (ii) a relatively high electron-hole recombination rate limits the transport of photoexcited carriers.⁶

One way of reducing the band gap for the next generation of TiO_2 -based photocatalysts is to combine multiple anions or cations to form ternary oxides. There are several possibilities for modifying TiO_2 to achieve band gap reduction using this approach: by replacing oxygen atoms with anions having a higher $2p$ orbital energy (such as B, C and N),^{7,8} by replacing Ti atoms with heavy metal ns^2 cations (such as Sn, Sb, Pb, or Bi) because of participation of $5s$ or $6s$ lone pairs in chemical bonding with the O $2p$ states,⁹⁻¹¹ by replacing Ti (which is formally a $3d^0$ metal in this circumstance) with $3d^n$ and $4d^n$ cations (such as V, Cr, Nb, or Mo),^{12,13} and by replacing Ti ($3d^0$) atoms with $3d^{10}$ cations (such as Zn, Cd, or Ga) inducing O $2p$ - cation $3d^{10}$ repulsion.¹⁴

The latter possibility can be achieved, for instance, by doping TiO_2 with ZnO, or through the formation of the ternary oxide ZnTiO_3 . Of the approaches mentioned above, this technique is also of interest since the coupling of TiO_2 with ZnO may achieve a more efficient electron-hole pair separation under illumination and, consequently, a higher reaction rate.¹⁵

We have previously found evidence that the band gaps of ternary oxides containing Ti and lone pair cations (Sn, Pb, Bi) could be predicted from the stoichiometric average of the band gaps of rutile TiO_2 and the lone pair oxide — despite the distinct crystal structure of the ternary oxide.¹¹ In this regard, it is worth investigating whether the electronic structure of ternary ZnTiO_3 can be thought of as an mix of the electronic structures of ZnO and TiO_2 (i.e. treating ZnTiO_3 as a $(\text{ZnO})(\text{TiO}_2)$ alloy). The most common natural phase of ZnTiO_3 is the rhombohedral “ilmenite” structure,¹⁶ although a cubic perovskite phase also exists.¹⁷ Structurally the two materials are fairly similar, the main difference being that the Ti-O_6 octahedra in hexagonal ZnTiO_3 are arranged in layers, rather like the layers in rutile TiO_2 (as shown in Fig. 1), while in cubic ZnTiO_3 the Ti-O_6 octahedra are arranged in a 3D network, rather like the arrangement in anatase TiO_2 .¹⁸ In the present manuscript we will examine the electronic structure of hexagonal ZnTiO_3 , which also has a structural similarity to wurtzite ZnO (as shown in Fig. 1 hexagonal ZnTiO_3 has a hexagonal plane of Zn ions, similar to the structure of wurtzite ZnO).

If the electronic structure of ZnTiO_3 does follow the trend previously found for lone pair/Ti ternary oxides, this suggests that the band gap for ZnTiO_3 should be halfway in between the band gaps of wurtzite ZnO and rutile TiO_2 . Since ZnO has an even higher band gap than TiO_2 , of 3.3 — 3.4 eV,¹⁹⁻²¹ this suggests that ZnTiO_3 might have a gap of about 3.2 eV which is even worse for optical photocatalysis than TiO_2 . However ZnTiO_3 is still worth study in this regard because if the electronic structure of this ternary oxide can be easily predicted from the electronic structures of the constituent oxides then the behaviour of other Ti- nd^{10} ternary oxides might be similarly predicted, and other nd^{10} binary oxides, like CdO and HgO, have smaller band gaps than TiO_2 .²²⁻²⁴

To investigate the electronic structure of ZnTiO_3 , we have performed density functional theory (DFT) calculations, X-ray photoelectron spectroscopy (XPS) measurements of the valence band, and X-ray emission and absorption spectroscopy (XES and XAS, respectively) measurements probing the occupied and unoccupied states, respectively. Our XES and XAS measurements were performed for the oxygen K , Ti $L_{2,3}$ and Zn $L_{2,3}$ edges of ZnTiO_3 , and the oxygen K edge of rutile TiO_2 , and wurtzite ZnO.

II. EXPERIMENTAL AND THEORETICAL METHODS

The ZnTiO_3 crystals were obtained from a zinc titanate precursor which was synthesized from layered titanate colloid with ZnO nanocrystals via the chemical bath deposition process. This reaction was conducted by mixing 2.2 grams of a layered (tetramethyl)ammonium titanate solution with a solution containing 6.5 g (25 mmol) of $\text{Zn}(\text{NO}_3)_2 \cdot 4\text{H}_2\text{O}$ and 3.5 g (25 mmol) (hexamethylene)tetramine $(\text{CH}_2)_6\text{N}_4$ in 50 mL of water. The zinc titanate precursor, obtained as a precipitate, undergoes profound changes under the influence of elevated temperatures in normal atmospheric conditions and allowed to obtain zinc titanate ZnTiO_3 with a rhombohedral symmetry at 900 ° C. The detailed description of performed synthesis and structural evolution of the ZnTiO_3 precursor at elevated temperatures as seen by XRD analysis as well as dielectric characterization of final product are described by in a previous paper.²⁵ Wurtzite ZnO and rutile TiO_2 powders were obtained from a commercial vendor (Alfa Aesar, 99.9% purity).

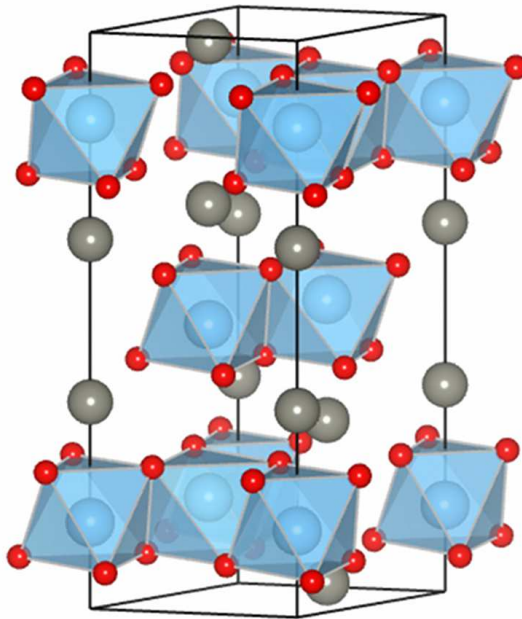


FIG. 1. Crystal structure of ZnTiO_3 . The Zn atoms are the isolated grey spheres, the Ti atoms are the blue spheres at the centre of octahedra coordinated by 6 oxygen atoms, represented by small red spheres. The unit cell is denoted by the black lines, the c axis is the longest axis, running up the length of the page. (Color online.)

Soft X-ray emission and absorption spectroscopy measurements were conducted at the Advanced Light Source (ALS) at the Lawrence Berkeley National Laboratories (Berkeley, CA, USA) and at the Canadian Light Source (CLS) at the University of Saskatchewan (Saskatchewan, SK, Canada), respectively. A Rowland circle geometry X-ray spectrometer with spherical gratings and an area sensitive detector was used at Beamline 8.0.1 at the ALS to collect the X-ray emission spectra,²⁶ while a channel plate fluorescence detector on the spherical grating monochromator beamline at the CLS was used to collect the X-ray absorption spectra in bulk-sensitive total fluorescence yield (TFY) mode.²⁷ The measurement resolution was about 10^3 and 2×10^3 for the emission and absorption measurements, respectively. All absorption spectra were normalized to the incident photon current using a highly transparent gold mesh in front of the sample to correct for intensity fluctuations in the incident photon beam, all emission spectra were acquired with an excitation energy far above resonance (475 eV for the Ti $L_{2,3}$ edges, 550 eV for the O K edge, and 1080 eV for the Zn $L_{2,3}$ edges). The ZnTiO_3 crystal and reference samples were affixed to a sample plate, placed under ultrahigh vacuum ($\sim 10^{-7}$ - 10^{-8} torr), and measured without any further preparation. The relative calibration between XES and XAS measurements was checked by exciting near resonance and observing the energy of the elastic scatter in the XES spectrometer.

XPS measurements were carried out with a high spatial- and energy-resolution PHI XPS Versaprobe 500 spectrometer (ULVAC-Physical Electronics, USA, 2011). This spectrometer uses a classic x-ray optic scheme with spherical quartz monochromator and energy analyzer working in the range of binding energies from 0 to 1500 eV, and has an electrostatic focusing system and magnetic screening. The energy resolution achieved was $\Delta E \leq 0.5$ eV with an Al $K\alpha$ source, the spot size was 200 μm . A dual-channel neutralizer was used in order to compensate the local charging of the sample under study due to the loss of photoelectrons. All samples under study were previously kept in the vacuum chamber for 24 hours under rotary pumping, and were measured at a pressure of 10^{-7} Pa. Typical signal to noise ratios were not less than 5000. The spectra were processed using ULVAC-PHI MultiPak Software 9.2 and the residual background was removed with the help of Tougaard method.²⁸ The XPS spectra were calibrated relative to the reference energy value of the carbon $1s$ core-level at 284.5 eV.²⁹

Density functional theory (DFT) calculations were performed using the experimental crystal structures of ZnTiO_3 ,³⁰ ZnO ,³¹ and TiO_2 .³² The full-potential linearized augmented plane wave (FP-LAPW) method was used, implemented by the WIEN2k code.³³ We used convergence and basis set parameters that are typical for these sort of systems.³⁴ To investigate the chemical activity of the Zn $3d^{10}$ shell, we used several different exchange-correlation potentials: Perdew, Burke, and Enzerhof's generalized gradient approximation (PBE),³⁵ the PBE functional with an on-site Coulomb potential of $U = 8$ eV for the Zn $3d$ states (PBE+ U),³⁶ and a hybrid functional (HF) based on PBE and

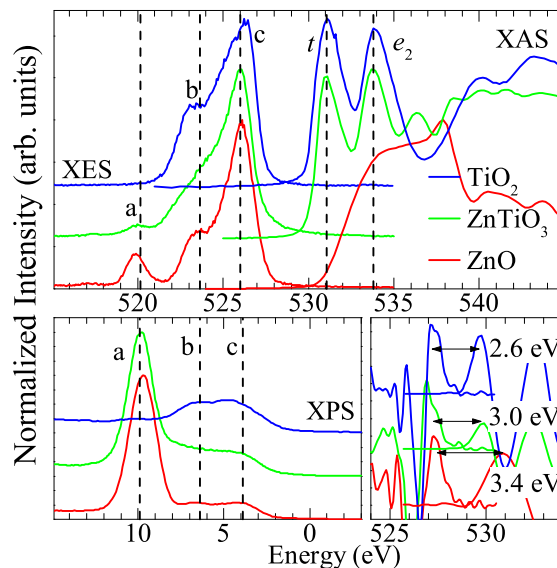


FIG. 2. Comparison of the X-ray spectra of ZnTiO_3 with TiO_2 and ZnO . The O K XES and XAS spectra for TiO_2 (rutile), ZnTiO_3 , and ZnO is in the top panel, the valence XPS spectra for the three compounds is in the bottom left panel, and the second derivatives of the oxygen K XES and XAS spectra are in the bottom right panel. The band gaps, estimated from the second derivatives, are also shown in the bottom right panel. (Color online.)

the Fock exchange using a typical 0.35 mixing.³⁷ To help calculate accurate band gaps, the modified Becke-Johnson (mBJ) potential was applied to the PBE and PBE+ U calculations (henceforth denoted as mBJ and mBJ+ U).³⁸

The XES and XAS spectra were also simulated from the DFT calculations by multiplying the partial densities of states with the dipole transition probability, implemented in the “XSPEC” package of WIEN2k.³⁹ For the XAS spectra a completely separate calculation with an explicit vacancy in the appropriate core level (O $1s$, Ti $2p_{3/2}$, or Zn $2p_{3/2}$) was performed. For these calculations a primitive $2 \times 2 \times 2$ supercell was used for ZnTiO_3 , and a primitive $3 \times 3 \times 3$ supercell was used for TiO_2 and ZnO . The calculated X-ray spectra were broadened with a Voigt function to mimic the experimental resolution and life-time broadening.

III. RESULTS AND DISCUSSION

Whether the electronic structure of ZnTiO_3 can be extrapolated from the electronic structures of ZnO and TiO_2 hinges in part on whether the X-ray spectra from ZnTiO_3 show features common with each of the constituent binary oxides. Indeed, since XES and XPS measurements of weakly correlated materials effectively probe the ground state partial and total occupied density of states (DOS), these spectroscopic techniques provide an ideal tool for studying the bulk electronic structure of these materials. Due to the influence of the final state on the X-ray spectrum, XAS provides a probe of the partial unoccupied DOS that is perturbed by the presence of a core hole (and therefore is not the true ground state DOS), however we have previously established that in post-transition metal and alkaline oxides the core hole often has a weak influence on the O $2p$ unoccupied DOS, and that the O K XAS is a reasonable approximation of the ground state unoccupied DOS in these systems.²² Although many transition metal oxides do exhibit a larger core-hole effect on the O K XAS, these spectra are still useful for analyzing the unoccupied O $2p$ DOS.⁴⁰

With that in mind, the O K XES, XAS and valence XPS of ZnTiO_3 , wurtzite ZnO , and rutile TiO_2 shown in Fig. 2 is encouraging. The O K XES of ZnTiO_3 shows hybridization between the O $2p$ states and the Zn $3d$ states at the bottom of the valence band, labelled as feature **a** in Fig. 2, and it is clear that the same hybridization occurs in ZnO at essentially the same energy. The large number of states present in the valence XPS confirms that this is the energy of the Zn $3d^{10}$ shell. The O K XES of ZnO and TiO_2 show a hybridization feature labelled as **b** in Fig. 2 that is also at essentially the same energy. In TiO_2 this feature was attributed to O $2p$ -Ti $3d$ hybridization,¹¹ while in ZnO it was attributed to O $2p$ -Zn $3d$, $4s$ hybridization.²² Near the valence band maximum, the XES spectrum for ZnTiO_3 , ZnO , and TiO_2 all have a maximum at roughly the same energy (labelled as **c** in Fig. 2), this can be attributed to the bulk of the O $2p$ states. These valence features are also present in the valence XPS. Since the O K XES probes only

the occupied states of $2p$ -character local to an oxygen site one can attribute the differences in intensities between the XPS and XES features as related to the hybridization strength of the O $2p$ states at those energies. This difference should only be considered qualitative, however, since the transition matrix elements for XES varies with energy,³⁹ and therefore the relative magnitudes at the valence band maximum and deeper in the valence band are not entirely proportional to the partial DOS at those energies.

We would like to stress that our XPS VB spectra should only be interpreted insofar as they agree with the XES O K spectra. We were not able to cleave the samples *in situ* for the XPS measurements, and the absence of surface contamination cannot be guaranteed. Since Zn is fully oxidized in both ZnTiO₃ and ZnO, we are justified in using the Zn $3d^{10}$ shell for alignment with the XES measurements (at least within an accuracy of 0.2 eV), but one should not use our XPS spectra for more detailed analysis of these materials.

The O K XAS spectrum of ZnTiO₃ and TiO₂ shown in Fig. 2 are both quite similar; this is again expected since the Ti $3d^0$ states should dominate the conduction band. The O K XAS spectrum is therefore dominated by two peaks which can be attributed (in a simple approximation) to O $2p$ hybridization with t and e_g symmetry $3d$ states.⁴¹ Since ZnO has no unoccupied $3d$ states these features do not occur in the O K XAS spectrum of ZnO.

Since the XES and XAS measurements provide independent probes of the occupied and unoccupied states with respect to the same core level energy, if the unoccupied core level causes only a minor perturbation to the unoccupied states in the XAS measurement then the two spectra can be used to estimate the band gap to within a few tenths of an eV. We have previously found that using the peaks in the second derivatives of the O K XES and XAS spectra to denote the band edges provides a reasonably accurate estimate of the band gap,²² although there is no theoretical justification for this technique. Using this technique on ZnTiO₃ suggests that the band gap is 3.0 ± 0.2 eV, as shown in Fig. 2, which is indeed in between the estimated gaps for TiO₂ (at 2.6 ± 0.2 eV) and ZnO (at 3.4 ± 0.2 eV). This analysis of the O K XES and XAS, and valence XPS measurements of ZnTiO₃ support the postulate that the electronic structure of ZnTiO₃ can be deduced from the electronic structures of ZnO and TiO₂.

There is clearly a problem with our band gap estimates, however. Although the estimated gap for wurtzite ZnO, at 3.4 ± 0.2 eV, is within error of the values of 3.3 - 3.4 eV quoted in the literature,¹⁹⁻²¹ the estimated for rutile TiO₂ is smaller than the value of about 3.0 eV quoted in the literature.⁴ This immediately suggests that O $1s$ core hole causes a significant shift (of about 0.4 eV) in the onset of the O K XAS with respect to the true ground state conduction band (while such a shift is obviously negligible in ZnO), however what (if any) is the core hole shift in O K XAS ZnTiO₃? To answer this, we must explicitly calculate the electronic structure of ZnTiO₃.

Calculating the electronic structure of materials involving transition metals with DFT is often notoriously difficult due to correlation effects involving the $3d$ electrons. However since in the materials studied herein the transition metals are either formally in the $3d^0$ or $3d^{10}$ ground state, neither TiO₂, ZnO, or ZnTiO₃ is a strongly correlated material, and one may anticipate that a simple DFT approach may accurately calculate the valence and conduction bands of ZnTiO₃.⁴²

The partial DOS of ZnTiO₃ for five different choices of exchange-correlation functional is shown in Fig. 3. These exchange-correlation functionals may be divided into three categories: the simple case (labelled as PBE and mBJ in Fig. 3), the hybrid functional case (HF), and the simple cases including a Hubbard potential U (PBE+ U , mBJ+ U). We stress that the mBJ calculation is primarily for computing an accurate band gap, the PBE (or PBE+ U) calculation will provide more accurate shapes for the valence and conduction bands. From Fig. 3 we can see that the simple DFT approach (PBE, mBJ) fails to isolate the Zn $3d^{10}$ states into the localized shell at the bottom of the valence band as observed in the O K XES and valence XPS. Both the hybrid functional and Hubbard potential methods do predict an isolated $3d^{10}$ shell for Zn, suggesting that p - d repulsion between the O $2p$ and Zn $3d$ states is underestimated in the simple DFT approach. Other than that all calculations are quite similar; the conduction band is dominated by Ti $3d$ states in two narrow bands, agreeing — at least qualitatively — with the measured O K XAS in Fig. 2 and there is partial occupation of the Ti $3d$ states in the valence band that hybridize with O $2p$ states between -5 and -3 eV (this is in agreement with feature **b** in Fig. 2). From these data we will use the PBE+ U calculation to assist in the analysis of the XES spectra, the PBE calculation (with a core-hole perturbation) to assist in the analysis of the XAS spectra, and the mBJ calculation as the “best” calculated band gap. The other data are shown here only for completeness.

The calculated band gaps of ZnTiO₃ are quite large: even in the PBE calculation (which is known to significantly underestimate band gaps⁴³) the gap is calculated to be 3.08 eV, and it is larger in all other calculation schemes (3.81 eV, 3.19 eV, 3.27 eV, and 4.14 eV in the mBJ, HF, PBE+ U , and mBJ+ U calculation schemes, respectively). This is striking because the calculated band gap for TiO₂ is 2.67 with the mBJ functional,¹¹ and the gap for ZnO is also less than that of ZnTiO₃ (0.82 eV, 2.75 eV, 1.17 eV, 1.48 eV, and 3.68 eV for PBE, mBJ, HF, PBE+ U , and mBJ+ U calculation schemes, respectively); implying that ZnTiO₃ has a larger band gap than ZnO and TiO₂. In fact, the optical band gap of ZnTiO₃ is 3.75, further supporting these calculations.⁴⁴ We note that the large calculated gap for ZnTiO₃ agrees with a value of 3.11 eV found in the literature⁴² (using a pseudopotential code), and the gap changes by 0.1 eV or less if we perform the calculation using different experimental or theoretically optimized

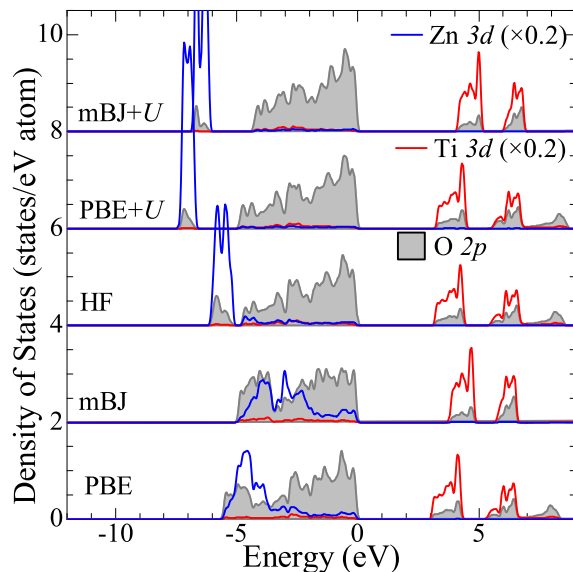


FIG. 3. Calculated DOS for ZnTiO_3 using several different exchange-correlation functionals. The valence band maximum is at 0 eV. Note that the amount of hybridization in the Zn $3d$ states is greatly influenced by the choice of functional, and further note that the shape of the conduction band is relatively insensitive to the choice of functional (Color online.)

lattice parameters⁴² or double or quadruple the number of k -points in our calculation, and we further note that the optical band gap of cubic ZnTiO_3 is 3.7,⁴⁵ supporting the idea that local structure is more important than long range symmetry in defining the bulk electronic structure of a material.

The DOS calculated with the PBE+ U scheme does a good job of reproducing the measured XES from the O K edge, Ti $L_{2,3}$ edge, and Zn $L_{2,3}$ edge, as shown in Fig. 4. This is an important verification of the calculated DOS, and supports the previous description of hybridization features in the O K XES described in Fig. 2. The calculated XES provides a method of deducing where the valence band maximum is in the measured XES — this is particularly valuable for the Ti and Zn $L_{2,3}$ XES where the overlap of the L_2 and L_3 levels in the former and the relatively weak amplitude near the top of the valence band in the latter make it otherwise difficult to determine the valence band maximum. It is clear from Fig. 4 that the bottom of the valence band is defined by Zn $3d$ - O $2p$ hybridized states, the middle of the valence band is defined by Zn $3d$, $4s$ - Ti $3d$ - O $2p$ hybridized states, and the top of the valence band is primarily due to O $2p$ states alone.

Since the calculated DOS provides an accurate basis for the measured XES spectra, why is the onset of the measured O K XAS spectrum of ZnTiO_3 in between those of ZnO and TiO_2 when the band gap of ZnTiO_3 is significantly larger than both? To investigate this we calculate the XAS spectra of ZnTiO_3 with a core hole explicitly included in the appropriate absorbing atom. This core hole perturbs the potential of the absorbing atom and can have two simple and simultaneous effects: the valence band maximum (relative to the binding energy of the fully occupied core level) and the band gap can both change (typically both will be lowered). The calculated and measured O K , Ti $L_{2,3}$, and Zn $L_{2,3}$ XAS spectra for the PBE calculation scheme are shown in Fig. 5 (note that the PBE scheme was used because the shape of the conduction band is essentially the same as that in the PBE+ U scheme, and the PBE scheme is much less computationally intensive). As in Fig. 4, the valence band maximum for each edge is shown by the dotted line, however it is important to note that each valence band maximum is fundamentally different as each relates to the DOS with a particular type of core hole.

From Fig. 5 we can see that the calculated XAS is in good agreement with the measurements (note that the Ti $L_{2,3}$ XAS includes multiplet effects that are not expected to be reproduced in a DFT calculation — in particular the two sharp features near 455 eV). It is also important to note that although each XAS spectrum has two sharp features near the edge related to the t and e_g splitting of the Ti $3d$ states, the influence of the core hole can cause different amounts of energy shift in these features relative to the Ti $3d$ states from the non-core-hole sites. Note that particular DOS related to the XAS spectrum is shown in grey in Fig. 5, while the total unoccupied Ti $3d$ states (including, for the Ti $L_{2,3}$ XAS, the single Ti site that is perturbed by the core hole) is shown in blue. Comparing these spectra with the DOS and band gap for the PBE calculation, we see that the net effect of the core hole is to shift the onset of the XAS to lower energies by 0.76 eV for the O K edge, 2.10 eV for the Ti L_3 edge, and 0.48 eV for the Zn L_3 edge.

Encouragingly, the same calculation for ZnO and TiO_2 predict a core hole shift of about 0.07 eV and 0.37 eV for

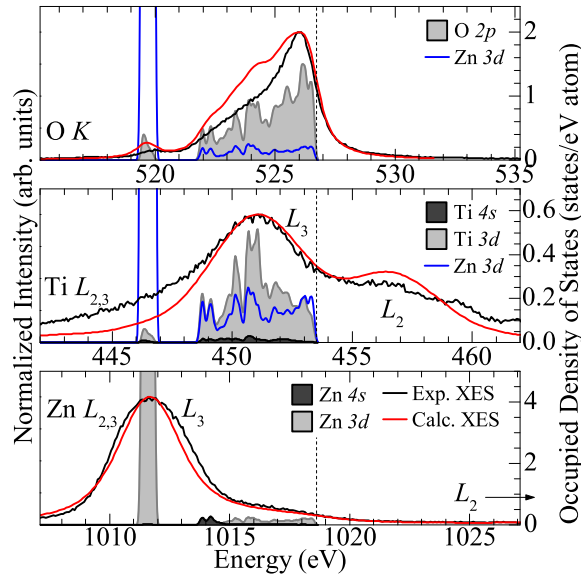


FIG. 4. The measured and calculated O K , Ti $L_{2,3}$, and Zn $L_{2,3}$ XES spectra. The calculated spectra made use of the PBE+ U exchange correlation functional, these spectra are also compared to the ground state DOS. For the O K and Ti $L_{2,3}$ spectra the Zn $3d$ states are also plotted for reference. Note the difference in spin-orbit splitting between the Ti L_2 and L_3 edges (in both the calculated and measured spectra the two edges overlap) and between the Zn L_2 and L_3 edges (for the heavier Zn the edges are separated by about 15 eV, the Zn L_2 is past the end of the x-axis). In DFT calculations, the states responsible for the L_2 edge are the same as those responsible for the L_3 edge, therefore the DOS is only shown once at the L_3 edge. The valence band maximum for the K or L_3 edge (as appropriate) is denoted by the dotted line in each panel. (Color online.)

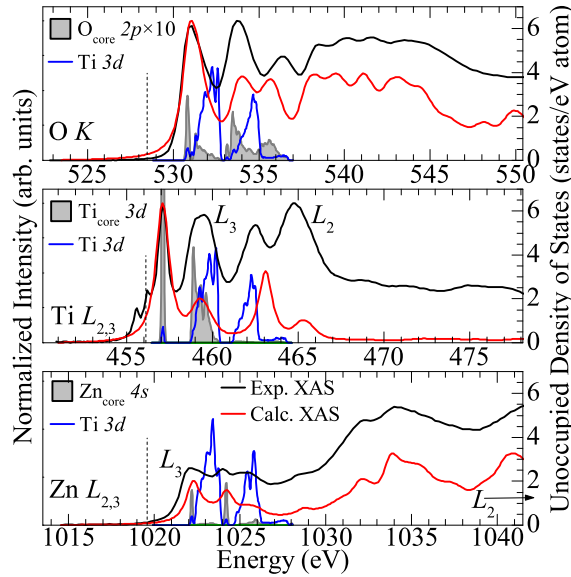


FIG. 5. The measured and calculated O K , Ti $L_{2,3}$, and Zn $L_{2,3}$ XAS spectra. The calculated spectra made use of the PBE exchange correlation functional, these spectra are also compared to the core-hole perturbed DOS. The presence of a core-hole on different atomic sites makes each XAS spectrum a unique calculation. In all cases the bulk Ti $3d$ states are plotted for comparison (note that the Ti $L_{2,3}$ absorption only involves a single core hole on one of 24 Ti atoms). The origin, relative amplitudes, and splitting of the Ti and Zn L_2 and L_3 edges are the same as described for Fig. 4. The valence band maximum for the K or L_3 edge (as appropriate) is denoted by the dotted line. (Color online.)

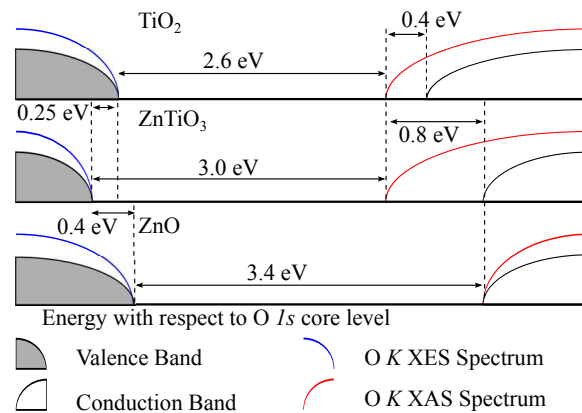


FIG. 6. A schematic view of the band gap and the O *K* XES and XAS spectra for TiO₂, ZnTiO₃, and ZnO. The valence and conduction bands are aligned with respect to the O 1s core level for each material. Here we assume that the conduction level of ZnTiO₃ is the same as that in ZnO, but the core hole shift in ZnTiO₃ is sufficient to bring the O *K* XAS to the same level as that in TiO₂. Reduced O *2p* - Zn *3d* repulsion reduces the valence band maximum in ZnTiO₃ with respect to that of ZnO; this is the primary mechanism behind the wider band gap in ZnTiO₃ compared to ZnO. (Color online.)

the O *K* XAS, respectively. If the second derivative gaps estimated in Fig. 2 are increased by this calculated core hole shift, the new band gaps are estimated as 3.47, 2.97, and 3.76 eV for ZnO, TiO₂, and ZnTiO₃, respectively — all within about 0.1 eV of the reported band gaps. In these circumstances the second derivative method does appear to accurately predict the band edges, however in materials where there is a significant core hole effect the edge of the XAS may not be near the ground state conduction band. From this perspective we can tentatively describe the mechanism behind the band gap broadening in ZnTiO₃: as in previous ternary oxides, the conduction band edge is determined by the TiO₆ octahedra, while the valence band edge is determined by the remaining cation-oxygen components.¹¹ However in the case of ZnTiO₃, the presence of the Ti sites reduces the O *2p* - Zn *3d* repulsion, and lowers the valence band maximum relative to ZnO. We would like to note that the core hole shift of 0.07 eV for ZnO is a refinement of our previously reported value of 0.1.²² A slightly older study suggests a core hole shift of 1.0 eV in ZnO,⁴⁶ however this value was achieved by rigidly shifting the bands, rather than explicitly calculating the perturbed band structure. Because the perturbed band structure often has a higher density of states closer to the conduction band minimum, a particular XAS spectral feature can be lower in energy than the corresponding ground state DOS feature either because the core hole shifts the onset of the conduction band minimum to lower energies, or shifts the DOS features closer to the conduction band minimum, or both. In the case of ZnO our calculations suggest that the latter case (the core hole perturbation shifts ground state DOS features closer to the conduction band minimum) is the most significant; there is only a very small shift in the onset of the conduction band.

This simple concept for reducing the valence band maximum in ZnTiO₃ is supported by the second derivatives in Fig. 2. From Fig. 2 we see that the peak in the second derivative of the O *K* XES spectrum for ZnTiO₃ is about 0.25 eV lower than that of TiO₂, and about 0.4 eV lower than that of ZnO. Since the band gaps of TiO₂ and ZnO are well known, we can infer from the peaks in the second derivatives of the O *K* XAS that there is a core hole shift of about 0.4 eV for TiO₂ and a negligible shift in ZnO. From this we can build a simple model for the band gap in ZnTiO₃, which is shown schematically in Fig. 6.

In this model we assume that while the Ti *3d*⁰ states largely define the character of the conduction band, the actual energy of the conduction band is set by Zn *4s* - O *2p* antibonding, and is therefore coincident in energy with the conduction band of ZnO. The presence of Ti-O bonding in ZnTiO₃ reduces the impact of O *2p* - Zn *3d* repulsion in ZnTiO₃ compared to ZnO, and is responsible for reducing the valence band maximum by 0.4 eV compared to ZnO, as seen in the second derivatives in Fig. 2. Simply adding this valence band maximum reduction to the gap of ZnO estimated by the second derivatives in Fig. 2 gives an estimate of 3.8 eV for the band gap of ZnTiO₃. During the XAS process, on the other hand, the core hole creates highly localized states near the absorbing O site. The TiO₂-like character of the conduction band becomes dominant at this point, and the core hole shift is sufficient to effectively reduce the O *K* XAS onset in ZnTiO₃ to that of TiO₂. This model is justified because while the energy gaps and shifts in Fig. 6 have been determined empirically (by the second derivatives in the O *K* XES and XAS spectra and the literature band gaps for ZnO and TiO₂), they are in good agreement with the calculated core hole shifts for TiO₂, ZnO, and ZnTiO₃ and the estimated band gap of ZnTiO₃ obtained through this process is quite close to the mBJ calculation (3.81 eV) and the optical gap (3.7 eV⁴⁵). We stress that the bands in Fig. 6 are aligned only with respect

to the oxygen $1s$ core level; our experimental data herein does not allow us to make accurate judgements on the band alignments with respect to the vacuum level or some other standard. Incidentally, a recently published study of transition metal doped ZnO films (Cr to Cu) also finds doping causes increased $p-d$ (and $s-d$) repulsion, resulting in a larger band gap.⁴⁷

In summary, we have studied the electronic structure of ZnTiO₃ with soft X-ray spectroscopy and DFT calculations. We have identified the hybridizations responsible for the spectral features in the O K XES and XAS, and the valence XPS in ZnTiO₃ and linked these to equivalent features in ZnO and TiO₂. We have found that a Hubbard U or a hybrid functional is necessary to accurately localize the Zn $3d^{10}$ shell in ZnTiO₃, which is similar to the case for ZnO.²² Our electronic structure calculations suggest that the band gap of ZnTiO₃ is between 3.8 and 4.1 eV (based on the two calculations involving the mBJ exchange-correlation functional) which is in reasonable agreement with the gap obtained by optical spectroscopy (3.7 eV⁴⁵), and with the gap between the peaks of the second derivatives of the measured XES and XAS spectra corrected with the calculated core hole shift (3.76 eV). We also find evidence that the TiO₆ octahedra in ZnTiO₃ reduce the O $2p$ - Zn $3d$ repulsion, resulting in a narrower valence band and a lower valence band maximum relative to that in ZnO.

From this analysis we suggest that the band gaps of ternary oxides formed by transition metal d^0 and d^{10} binary oxide precursors may be estimated from O K XES and XAS measurements of the ternary and parent binary oxides as follows:

1. Estimate the band gap of the d^{10} binary oxide by taking the difference between the peaks in the second derivatives of the O K XES and XAS measurements.
2. Estimate the change in the valence band maximum from reduced $p-d$ repulsion by taking the difference between the peaks in the second derivative of the O K XES of the d^{10} binary oxide and the ternary oxide.
3. Estimate the band gap of the ternary oxide by adding the difference between the valence band maxima to the estimated gap of the d^{10} binary oxide.

This procedure, and the identification described above, may be helpful for analyzing X-ray spectra from more complicated oxides, or even complex heterostructures based on d^{10} and d^0 parent oxides. This analysis also suggests that band gap reduction of TiO₂ may be possible via alloying with a lower band gap d^{10} oxide such as CdO or HgO,²² and suggests a method for band gap engineering in these types of materials.

ACKNOWLEDGMENTS

We gratefully acknowledge support from the Natural Sciences and Engineering Research Council of Canada (NSERC) and the Canada Research Chair program. This work was done with partial support of Ural Division of Russian Academy of Sciences (Project 12-I-2-2040). The Advanced Light Source is supported by the Director, Office of Science, Office of Basic Energy Sciences, of the U. S. Department of Energy under Contract No. DE-AC02-05CH11231. The Canadian Light Source is supported by NSERC, the National Research Council (NSC) Canada, the Canadian Institute of Health Research (CIHR), the Province of Saskatchewan, Western Economic Diversification Canada, and the University of Saskatchewan. The computational part of this research was enabled by the use of computing resources provided by WestGrid and Compute/Calcul Canada. Finally, the technical support of ULVAC-Physical Electronics company and Mr. Ken Wasness is gratefully acknowledged.

* Contact Author: john.mcleod@usask.ca

¹ K. Hashimoto, H. Irie, and A. Fujishima, Jpn. J. Appl. Phys. **44**, 8269 (2005).

² A. Fujishima and K. Honda, Nature **238**, 37 (1972).

³ R. Asahi, T. Morikawa, T. Ohwaki, K. Aoki, and Y. Taga, Science **293**, 269 (2001).

⁴ J. Pascual, J. Camassel, and H. Mathieu, Phys. Rev. Lett. **39**, 1490 (1977).

⁵ H. Tang, H. Berger, P. E. Schmid, and F. Lévy, Solid State Commun. **92**, 267 (1994).

⁶ H. Wang and J. P. Lewis, J. Phys.: Condens. Matter **18**, 421 (2006).

⁷ H. Irie, Y. Watanabe, and K. Hashimoto, J. Phys. Chem B **107**, 5483 (2003).

⁸ S. Khan, M. Al-Shahry, and W. B. Ingler Jr., Science **297**, 2243 (2002).

⁹ A. Walsh, SPIE Newsroom: Solar & Alternative Energy, 1 (2009).

¹⁰ J. Moon, H. Takagi, Y. Fujishiro, and M. Awano, J. Mater. Sci. **36**, 949 (2001).

¹¹ J. A. McLeod, R. J. Green, E. Z. Kurmaev, N. Kumada, A. A. Belik, and A. Moewes, Phys. Rev. B **85**, 195201 (2012).

¹² T. Umebayashi, T. Yamaki, H. Itoh, and K. Asai, J. Phys. Chem. Sol. **63**, 1909 (2002).

- ¹³ Y. Yang, X.-J. Li, J.-T. Chen, and L.-Y. Wang, *J. Photochemistry and Photobiology A: Chemistry* **163**, 517 (2004).
- ¹⁴ A. Schleife, F. Fuchs, J. Furthmüller, and F. Bechstedt, *Phys. Rev. B* **73**, 245212 (2006).
- ¹⁵ G. Marci, V. Augugliaro, M. J. López-Muñoz, C. Martín, L. Palmisano, V. Rives, M. Schiavello, R. J. D. Tilley, and A.-M. Venezia, *J. Phys. Chem. B* **105**, 1026 (2001).
- ¹⁶ O. Yamaguchi, M. Morimi, H. Kawabata, and K. Shimizu, *J. Am. Ceram. Soc.* **70**, C97 (1987).
- ¹⁷ W.-J. Yin, S.-H. Wei, M. M. Al-Jassim, and Y. Yan, *Phys. Rev. B* **85**, 201201(R) (2012).
- ¹⁸ U. Steinike and B. Wallis, *Cryst. Res. Technol.* **32**, 187 (1997).
- ¹⁹ Ü. Özgür, Y. I. Alivov, C. Liu, A. Teke, M. A. Reshchikov, S. Doğan, V. Avrutin, S.-J. Cho, and H. Morkoc, *J. Appl. Phys.* **98**, 041301 (2005).
- ²⁰ V. Srikant and D. R. Clarke, *J. Appl. Phys.* **83**, 5447 (1998).
- ²¹ C. Klingshirn, *Phys. Stat. Sol.* **71**, 547 (1975).
- ²² J. A. McLeod, R. G. Wilks, N. A. Skorikov, L. D. Finkelstein, M. Abu-Samak, E. Z. Kurmaev, and A. Moewes, *Phys. Rev. B* **81**, 245123 (2010).
- ²³ P.-A. Glans, T. Learmonth, K. E. Smith, J. Guo, A. Walsh, G. W. Watson, F. Terzi, and R. G. Egdell, *Phys. Rev. B* **71**, 235109 (2005).
- ²⁴ N. Ueda, H. Maeda, H. Hosono, and H. Kawazoe, *J. Appl. Phys.* **84**, 6174 (1998).
- ²⁵ I. Bobowska, A. Opasińska, A. Wypych, and P. Wojciechowski, *Mat. Chem. Phys.* **134**, 87 (2012).
- ²⁶ J. J. Jia, T. A. Callcott, J. Yurkas, A. W. Ellis, and F. J. Himpsel, *Rev. Sci. Instr.* **66**, 1394 (1995).
- ²⁷ T. Regier, J. Krochak, T. K. Sham, Y. F. Hu, J. Thompson, and R. I. R. Blyth, *Nucl. Instrum. Meth. A* **582**, 93 (2007).
- ²⁸ S. Tougaard, *Solid State Commun.* **61**, 547 (1987).
- ²⁹ J. Moulder, W. Stickle, P. Sobol, and K. Bomben, Handbook of X-ray Photoelectron Spectroscopy, edited by J. Chastain (Perkin-Elmer Corporation, Minnesota, 1992).
- ³⁰ S. F. Bartram and R. A. Slepety, *J. Am. Cer. Soc.* **44**, 493 (1961).
- ³¹ K. Kinohara and G. Donnay, *The Canadian Mineralogist* **23**, 647 (1985).
- ³² R. J. Swope, J. R. Smyth, and A. C. Larson, *Am. Mineral.* **80**, 448 (1995).
- ³³ P. Blaha, K. Schwarz, G. K. H. Madsen, D. Kvasnicka, and J. Luitz, **WIEN2k**, An Augmented Plane Wave + Local Orbitals Program for (Karlheinz Schwarz, Techn. Universität Wien, Austria, 2001) ISBN 3-9501031-1-2.
- ³⁴ Energy convergence of 0.0001 Ryd, charge convergence of 0.001 e, the Brillouin zone discretized on a 1000-element k -point grid, $R_{min}^{MT} K_{max} = 7$, and atomic spheres chosen so they were nearly touching. See our previous papers for more detail.^{11,22}
- ³⁵ J. P. Perdew, K. Burke, and M. Ernzerhof, *Phys. Rev. Lett.* **77**, 3865 (1996).
- ³⁶ This potential was chosen *a posteriori* to shift the Zn $3d^{10}$ to the experimentally observed energies.⁴⁸
- ³⁷ F. Tran, P. Blaha, K. Schwarz, and P. Novák, *Phys. Rev. B* **74**, 155108 (2006).
- ³⁸ F. Tran and P. Blaha, *Phys. Rev. Lett.* **102**, 226401 (2009).
- ³⁹ K. Schwarz, A. Neckel, and J. Nordgren, *J. Phys. F: Metal Phys.* **9**, 2509 (1979).
- ⁴⁰ E. Z. Kurmaev, R. G. Wilks, A. Moewes, L. D. Finkelstein, S. N. Shamin, and J. Kuneš, *Phys. Rev. B* **77**, 165127 (2008).
- ⁴¹ F. M. F. de Groot, M. Grioni, J. C. Fuggle, J. Ghijsen, G. A. Sawatzky, and H. Petersen, *Phys. Rev. B* **40**, 5715 (1989).
- ⁴² X.-C. Zhang, C.-M. Fan, Z.-H. Liang, and P.-D. Han, *Acta Phys.-Chim. Sin.* **27**, 47 (2011).
- ⁴³ P. Dufek, P. Blaha, and K. Schwarz, *Phys. Rev. B* **50**, 7279 (1994).
- ⁴⁴ C. Ye, S. S. Pan, X. M. Teng, H. T. Fan, and G. H. Li, *Appl. Phys. A* **2008**, 375 (90).
- ⁴⁵ C. Ye, Y. Wang, Y. Ye, J. Zhang, and G. H. Li, *J. Appl. Phys.* **106**, 033520 (2009).
- ⁴⁶ A. R. H. Preston, B. J. Ruck, L. F. J. Piper, A. DeMasi, K. E. Smith, A. Schleife, F. Fuchs, F. Bechstedt, J. Chai, and S. M. Durbin, *Phys. Rev. B* **78**, 155114 (2008).
- ⁴⁷ S. J. Gilliland, J. A. Sans, J. F. Sánchez-Royo, G. Almonacid, B. García-Domene, A. Segura, G. Tobias, and E. Canadell, *Phys. Rev. B* **86**, 155203 (2023).
- ⁴⁸ T. Paudel and W. Lambrecht, *Phys. Rev. B* **77**, 205202 (2008).